

Citation for published version:

Zhang, D, Xu, S, Zhao, X, Qian, W, Bowen, CR & Yang, Y 2020, 'Wireless Monitoring of Small Strains in Intelligent Robots via a Joule Heating Effect in Stretchable Graphene–Polymer Nanocomposites', *Advanced Functional Materials*, vol. 30, no. 13, 1910809. <https://doi.org/10.1002/adfm.201910809>

DOI:

[10.1002/adfm.201910809](https://doi.org/10.1002/adfm.201910809)

Publication date:

2020

Document Version

Peer reviewed version

[Link to publication](#)

This is the peer reviewed version of the following article: Zhang, D., Xu, S., Zhao, X., Qian, W., Bowen, C. R., Yang, Y., Wireless Monitoring of Small Strains in Intelligent Robots via a Joule Heating Effect in Stretchable Graphene–Polymer Nanocomposites. *Adv. Funct. Mater.* 2020, 30, 1910809, which has been published in final form at <https://doi.org/10.1002/adfm.201910809>. This article may be used for non-commercial purposes in accordance with Wiley Terms and Conditions for Self-Archiving.

University of Bath

General rights

Copyright and moral rights for the publications made accessible in the public portal are retained by the authors and/or other copyright owners and it is a condition of accessing publications that users recognise and abide by the legal requirements associated with these rights.

Take down policy

If you believe that this document breaches copyright please contact us providing details, and we will remove access to the work immediately and investigate your claim.

Wireless monitoring of small strains in intelligent robots via a Joule heating effect in stretchable graphene-polymer nanocomposites

Ding Zhang^{1,3}, Suwen Xu¹, Xue Zhao¹, Weiqi Qian^{1,3}, Chris R. Bowen², and Ya Yang^{1,3,4}*

¹CAS Center for Excellence in Nanoscience, Beijing Key Laboratory of Micro-Nano Energy and Sensor, Beijing Institute of Nanoenergy and Nanosystems, Chinese Academy of Sciences, Beijing 100083, P. R. China.

²Department of Mechanical Engineering, University of Bath, BA27AK, UK.

³School of Nanoscience and Technology, University of Chinese Academy of Sciences, Beijing 100049, P. R. China.

⁴Center on Nanoenergy Research, School of Physical Science and Technology, Guangxi University, Nanning 530004, P. R. China.

*Correspondence and requests for materials should be addressed to Y. Y. (email: yayang@binn.cas.cn).

ABSTRACT: Flexible strain sensors are an important component for future intelligent robotics. However, the majority of current strain sensors must be electrically connected to a corresponding monitoring system via conducting wires, which increases system complexity and restricts the working environment for monitoring strains. Here, we report on stretchable graphene-polymer nanocomposites that act as a strain sensor using a Joule heating effect. When the resistance of the sensor changes in response to a strain, the resulting change in temperature is wirelessly detected in an intelligent robot. By engineering and optimizing the surface structure of graphene-polymer nanocomposites, the fabricated strain sensors exhibit excellent stability when subjected to periodic temperature signals over 400 cycles while being periodically strained and deliver a high strain sensitivity of $7.03 \times 10^{-4} \text{ } ^\circ\text{C}^{-1}/\%$ for strain levels of 0 to 30%. As a wearable electronic device, the approach provides a capability to wirelessly monitor small strains for intelligent robots at a high strain resolution of approximately 0.1%. Moreover, when the strain sensing system operates as a multi-channel structure, it allows precise strain detection simultaneously, or in sequence, for each finger of an intelligent robot.

KEYWORDS: wireless, strain sensor, joule heating effect, graphene-polymer, stretchable.

With the development of the field of intelligent materials and structures, flexible strain sensors figure prominently in applications related to health monitoring¹⁻⁴, electronic skins⁵⁻⁶, human-machine interfaces⁷⁻⁸, soft robotics⁹⁻¹⁰, and implantable electronics¹¹⁻¹³. However, the majority of reports on flexible strain sensors are committed to the improvement of flexibility, sensitivity, resolution, and cycle life. However, the need for existing strain sensors to be electrically connected to a corresponding monitoring system via conducting wires increases system complexity and restricts the working environment and condition of strain monitoring. Therefore, the investigation and realization of new wireless and remote strain detection methods is vital for broadening the application areas of flexible strain sensors. This is a key research challenge where there has been limited reported research to date.

To improve the performance of flexible strain sensors, a significant amount of research has explored the design and optimization of sensor structure, matrix material design and doping of the active materials. Polymer composites with conductive fillers have attracted the attention of researchers due to their simple structure and mature fabrication technologies. As an important example, inorganic-organic composites consisting of polymer matrices (such as polydimethylsiloxane, ecoflex, etc.) and conductive fillers (metal nanowires, carbon nanotubes, etc.) have been widely reported¹⁴⁻²², which often achieve strain detection through monitoring the change in ohmic resistance of the polymer composites with deformation. Moreover, graphene, a two-dimensional carbon material with extraordinary characteristics including remarkable thermal conductivity and electronic transport properties²³⁻²⁵, has attracted significant attention since its discovery in 2004²⁶. Graphene-polymer nanocomposites have exhibited outstanding performance in self-powered strain detection with excellent stretchability and electrical conductivity, and possess a mature technology to allow deposition of a thin graphene film on a stretchable ecoflex matrix through a vacuum filtration process²⁷⁻²⁹. There has been less research reporting on strain detection by monitoring other signals, such as current, capacitance, piezoelectric, and magnetoresistive signals^{27,30-32}. These studies have improved the performance of flexible strain sensors to some degree. However, they still require the uses of electrically conducting wires to connect the strain sensors to a control port of a monitoring system to detect the electrical signals in response to applied strains.

Here, we fabricate a graphene-ecoflex nanocomposite as a stretchable strain sensor with large dimension (35mm × 8mm), and realize wireless monitoring of small strains in intelligent robots based on a Joule heating effect via an applied external voltage. When the resistance of the sensor changes in response to a strain, the resulting change in temperature can be wirelessly detected. The fabricated strain sensor shows excellent stability with periodic temperature signals over 150 and 400 cycles under repetitive strains from 0 to 100% and 50%, respectively. With the aid of a laser engraving machine, a

high strain sensitivity of $7.03 \times 10^{-4} \text{ }^\circ\text{C}^{-1}/\%$ from 0 to 30% strain was achieved by engineering the heat transfer characteristics and optimizing the side length and depth of the carved graphene patterns on the surface structure of the strain sensor. We demonstrate that, as a wearable device, the material can be used to wirelessly monitor small strains in intelligent robots with a high strain resolution of approximately 0.1% by an infra-red (IR) camera. Furthermore, we also operate five identical strain sensors in a parallel connection to form a strain sensor system with a multichannel structure, and precisely realize strain detection of individual fingers of an intelligent robot simultaneously, or in sequence.

Results

Characterization of graphene sheet and graphene-ecoflex nanocomposite. Fig. 1a illustrates a scanning electron microscopy (SEM) image of the graphene used in this work and indicates a three-dimensional wrinkled structure with large lateral size. Fig. 1b shows a transmission electron microscopy (TEM) image of the initial graphene sheet, which indicates that the structure consists of few-layer graphene. The inset of Fig. 1b displays a high-resolution TEM image of regular hexagonal carbon atoms structure of graphene, and the estimated interplanar spacing is approximately 2.1 Å, corresponding to the (100) plane of hexagonal graphite (JCPDS No. 75-1621)^{27,33}. By using a controllable vacuum filtration process and control of the concentration and mass of graphene in an aqueous solution, we prepared graphene-ecoflex composite films of uniform thickness. As illustrated in Fig. 1c, wrinkled graphene sheets are formed on the upper surface of graphene-ecoflex nanocomposite film, which is created during the manufacture of the nanocomposite film. The cross-sectional SEM image, shown in the inset of Fig. 1c, confirms the bilayer graphene-ecoflex structure of the nanocomposite film and indicates that the graphene layers thickness is approximately 60 μm. All graphene-ecoflex specimens were cut to a dimension of 35 mm × 8 mm, and a detailed description of the fabrication process is provided in the Methods section. As seen from Fig. 1d, several deformation mechanisms of the original shape can be achieved, including torsion and tension, which indicates the excellent flexibility and stretchability of the manufactured sensors. To demonstrate the ability to sense strain as a result of a change in resistance of the nanocomposite film, the corresponding current-voltage (I-V) curves were initially characterized (Supplementary Fig. S1) by stretching the specimen with effective dimension of 20 mm × 8 mm from 0 to 100% strain; see inset of Fig. 1e. Then, the resistances at different levels of strain were obtained by calculating the results in Supplementary Fig. S1. Herein, the strain degree is defined as $\varepsilon = (l - l_0)/l_0 \times 100\%$, where l_0 and l are the original and stretched length of the graphene-ecoflex specimen, respectively. Through linear fitting, two fitting linear formulas are obtained:

$$\text{when } \varepsilon < 60\%, \quad R = 10.8\varepsilon + 0.79 \text{ (k}\Omega\text{)} \quad (1)$$

$$\text{and } 60\% \leq \varepsilon < 100\%, \quad R = 38.4\varepsilon + 0.79 \text{ (k}\Omega\text{)} \quad (2)$$

$$\text{which are both of the form:} \quad R = A\varepsilon + B \quad (3)$$

where R is the resistance of specimen, A , B are constants associated with the composites. The fitting results are consistent with a theoretical formula of previous research reports³⁴⁻³⁶:

$$R/R_0 = (l/l_0)^2 = (1 + \varepsilon)^2 = 1 + 2\varepsilon + \varepsilon^2 \quad (4)$$

Where R_0 is the initial resistance of specimen; when $\varepsilon \ll 1$, eq (4) can be expressed as

$$R/R_0 = 1 + 2\varepsilon \quad (5)$$

$$\text{Then} \quad R = 2R_0\varepsilon + R_0 \quad (6)$$

Considering the potential for slip between the graphene sheets on the surface of the ecoflex matrix when subjected to a relatively large strain, it is reasonable that the test result of eq (3) has some difference compared to the theoretical function eq (6). The gauge factor is defined as $(R - R_0)/(R_0\varepsilon)$ and increases from 13.4 to 26.6 at strain levels from 10% to 100%, as shown in Fig. 1f, which indicates the excellent strain sensing properties.

Joule heating property and cyclic stability of the stretchable strain sensor. For the graphene-ecoflex bilayer the application of strain will lead to a change in resistance, which corresponds to a change in temperature of the sensor during Joule heating. As a result, the change of sensor temperature can be monitored wirelessly with an IR camera to provide a route to realize wireless monitoring of strain. Therefore, the relationship between temperature and strain must be determined. As an important component of the wireless operation, the Joule heating behavior was initially investigated in detail by examining the relationship between temperature and the externally applied voltage. As seen from Fig. 2a, the time-dependent temperature variation of the film was recorded by an IR camera, with an externally applied voltage of 0, 2.5, 5.0, 7.5, 10.0, 12.5, 15.0, 17.5, 20.0 and 22.5 V on two sides of the film that was controlled by a direct current (DC) power system. From the temperature-voltage curve in Supplementary Fig. S2a, a stable temperature (T_s) increase from 0 to 93 °C was achieved with an increase of applied voltage under each stable state in equilibrium. The corresponding temperature distribution images were also recorded at the ten applied voltages described above, as shown in Supplementary Fig. S2b. In order to visualize the level of Joule heating, three graphene-ecoflex films were connected in parallel under an applied external voltage of 22.5 V and then attached to the outer surface of a small beaker that was filled with water, see Supplementary Fig. S3a. After several minutes, the temperature of the water and graphene-ecoflex film increased from 26 to 69 and 82 °C respectively,

as illustrated in Supplementary Fig. S3b and S3c, which suggests that the film can act as a flexible heater with high performance. Supplementary Fig. S4a demonstrates the stable temperature cycling stability of the graphene-ecoflex film over 120 cycles under the application of a periodic externally applied voltage of 22.5 V.

If the material is to act as a strain sensor, it is essential to explore the relationship between the sensor temperature and applied strain. Fig. 2b displays several temperature distribution images at different levels of applied strain under an applied voltage of 22.5 V. Fig. 2c indicates the temperature change for five different initial temperatures, including 93, 80, 70, 60 and 50 °C, which were all under an applied tensile strain from 0 to 100%. It can be seen that the higher the initial temperature, the faster the temperature decreases with an increase of strain, and Supplementary Fig. S4b presents the corresponding temperature-time curves at a stable state, where the temperature reaches to an equilibrium state.

As a result of these observations, an initial temperature of 93 °C was selected for the strain sensors to provide the greatest strain sensitivity. Fig. 2d displays three cycles of testing under consecutive processes of stretching/releasing at strain levels of 0-100%, where the temperature variation is consistent, as depicted Supplementary Fig. S5a. Furthermore, the periodic temperature signals were all almost reversible over 400 and 150 cycles under the application of repetitive strains from 0 to 50% and 100% respectively, as shown in Supplementary Fig. S5b and S5c. This data demonstrates the excellent stability of the fabricated wireless strain sensor based on a Joule heating effect. To illustrate the relationship between temperature and strain, and considering former resistance fitting functions eq (1) and (2), fitting was undertaken of the stable temperature (T_s) and strain at an initial temperature of 93 °C under a relatively small applied strain range from 0 to 50%, and the fitting formula is

$$T_s = 41.78/(\varepsilon + 0.437) - 2.6 \text{ (}^\circ\text{C)} \quad (7)$$

, as displayed in Fig. 2e.

According to Joule's law, the released electric power (P) is,

$$P = U^2/R \quad (8)$$

Where U represents the applied external voltage. The stable temperature of the sensor is proportional to the thermal power, and considering heat losses due to convection, conduction and radiation, we can approximate the stable temperature as,

$$T_s \propto U^2/R \quad (9)$$

Combining the fitting results of eq (3) above, for a fixed externally applied voltage U , we can determine T_s :

$$T_s = C/(A\varepsilon + B) + D \quad (10)$$

Where the C and D are constants and can be regarded as correction factors. It can be seen that the fitting function above is consistent with the derived form of eq (7).

Performance optimization of the stretchable strain sensor. As mentioned above, the stable temperature of the graphene-ecoflex film is directly affected by the synergistic effect of the released Joule heat and heat losses. Factors that influence the final equilibrium temperature including the applied external voltage, the surface structure and heat transfer of the materials, and other factors such as ambient temperature and airflow. As a result, the temperature of the sensor will be affected, thus affecting the properties of the strain sensor. For this reason, we further fabricated several graphene-ecoflex films with a range of surface graphene patterns on the ecoflex matrix using a laser engraving machine (Universal, PLS 4.75). Supplementary Fig. S6a presents a schematic of the working mechanism and the different surface morphologies of the strain sensors, where we explored the effect of surface morphology such as size and depth on the sensor equilibrium temperature. Supplementary Fig. S6b depicts the detailed fabrication process and, as illustrated in Fig. 3a, graphene square areas were carved out by the engraving process and peeled off from the surface of the graphene-ecoflex film, and the graphene-free areas were formed with side lengths of 0.5, 1.0, 1.5, 2.0 and 2.5 mm. The corresponding specimens are termed specimen-0.5, specimen-1.0, specimen-1.5, specimen-2.0, specimen-2.5 respectively. The total numbers of graphene-free areas with the side length from 0.5 mm to 2.5 mm are 189, 84, 36, 18 and 10, respectively. All graphene-free areas were calculated and it can be seen that the total graphene-free area of specimen-1.0 is 84 mm² which is larger than the other samples, as displayed Fig. 3b. Based on the relationship between temperature and applied voltage in eq (10), and to facilitate a comparison of the sensing performance of strain sensors with different surface morphologies, the initial temperatures were all maintained at ~90.5 °C by a controllable DC power system for the following research experiments.

Supplementary Fig. S7 illustrates a five-cycle test under consecutive process of stretching/releasing at strain levels of 0-100% for the six specimens above; here '0 mm' indicates the specimen without any laser engraving and a coherent graphene layer. It can be seen that the temperature variation of the strain sensors were all stable by the fifth cycle. Fig. 3c provides the temperature-strain curves of the six specimens based on the fifth cycle, and the temperature of specimen-1.0 decreases rapidly with strain compared with other specimens, which suggests that the performance of the strain sensor were affected

by engraving size. The corresponding temperature distribution images along with stretchable strain were also recorded in Supplementary Fig. S8. Linear fitting of the temperature-strain curves (Fig. 3c) was undertaken, along with linear fitting of curves between the reciprocal of temperature ($1/T$) and strain (ε) in Fig. 3d for the six specimens at strain levels from 0 to 30%. The dependent variable $1/T$ is linearly increasing with an increase of the independent variable ε and the slope of line in Fig. 3d is an indicator of the sensitivity of stretchable strain sensor, and specimen-1.0 and specimen-0 display the highest and the lowest sensitivities of 5.61×10^{-4} and $3.57 \times 10^{-4} \text{ } ^\circ\text{C}^{-1}/\%$, respectively. From the above experimental research, we have been able to optimize the best engraving size of 1.0 mm for graphene-ecoflex strain sensor to achieve the greatest change in temperature with strain.

Moreover, based on the optimum sensor engraving size of 1.0 mm, we have designed and fabricated an additional five strain sensors with different engraving depths, where the detailed fabrication process was similar to the schematic in Supplementary fig. S6b. A different depth was acquired by tailoring the engraving power and times. Supplementary Fig. S9a is a photograph of five specimens from left to right with an increase of engraving times, and these specimen show excellent stretch and torsion properties in Supplementary Fig. S9b. Supplementary Fig. S10 characterizes the engraving depth of 215, 230, 268, 293 and 308 μm using a profilometer (KLA-Tencor P7), and the corresponding specimen are termed specimen-1.0/215, specimen-1.0/230, specimen-1.0/268, specimen-1.0/293 and specimen-1.0/308 respectively. We have also studied the cyclic performance for strain sensing for five cycles with a temperature range from 90.5°C to room temperature, as shown in Supplementary Fig. S11a-e. It can be seen that the temperatures of these specimens had decreased to room temperature before reaching a strain level of 100%. Fig. 3e illustrates the temperature-strain curves of the five specimens based on the fifth cycle, and the temperature of specimen-1.0/268 decreases more quickly compared with other specimens, which suggests that the engraving depth directly affects the sensing performance of the strain sensor. Fig. 3f provides the linear fitting curves corresponding to Fig. 3e, the functions between the reciprocal of temperature ($1/T$) and strain (ε) were obtained through linear fitting of curves in Fig. 3e. The sensitivities increase from $4.97 \times 10^{-4} \text{ } ^\circ\text{C}^{-1}/\%$ of specimen-1.0/308 to $7.03 \times 10^{-4} \text{ } ^\circ\text{C}^{-1}/\%$ of specimen-1.0/268, and the linear fitting formula corresponding to specimen-1.0/268 is

$$1/T = (7.03 \times 10^{-4})\varepsilon / \% + 1/90.5 \quad (11)$$

Based on these observations we now select the optimized stretchable strain sensor as the key research object with the engraving side length of 1.0 mm and depth of 268 μm , and the strain resolution of the optimized sensor is subsequently studied. According to Supplementary Fig. S11f, when a periodic strain of 0.25% is applied to the strain sensor, we can see that the periodic strain can be detected precisely,

which indicates that strain resolution of the strain sensor is less than 0.25%.

Application for wireless monitoring intelligent robot. Flexible and stretchable strain sensors are widely used in modern society as intelligent monitoring devices. Here, we demonstrate a potential application of the stretchable strain sensor in wireless monitoring of the small motion of intelligent robots by using the optimized specimen-1.0/268 in terms of engraving size and depth. Through intelligent manipulation software, a freely moving manipulator was used in the subsequent strain detection tests. A stretchable strain sensor was attached to a finger joint position of the manipulator and an initial temperature of ~ 91.4 °C was achieved by a controllable direct current (DC) power system. We initially monitored the strain of a robot finger by measuring the temperature variation under seven motion states of the manipulator, as seen from Fig. 4a, where the insert is a photograph of the manipulator test device. We can see that the temperature of the strain sensor decreases to a stable state gradually with an increase of strain as a result of increase in degree of bending of the finger. In addition, the temperature increases gradually with a decreasing in strain during the recovery process. Under the same degree of bending of the finger, the temperatures of the sensor were almost the same during an increase and decrease of applied strain, indicating excellent cyclic stability and recovery properties. Fig. 4b and 4c show seven temperature distribution images and photographs of the manipulator, which all correspond to the seven bend states of the finger in Fig. 4a, respectively. Supplementary Fig. S12 displays the temperature variation corresponding to the bending of a finger from state 1 to 7 that leads to corresponding stable temperatures of 91.4 and 51.5 °C, and Supplementary Movie S1 records temperature variation images of partial cycles, which indicate the remarkable cyclic stability of the strain sensor over 100 cycles. In order to investigate the precise strain resolution of this strain sensor, within the limits of the experimental conditions available, an unknown and periodic strain was obtained by controlling the intelligent manipulation software. As seen from Supplementary Fig. S13, the corresponding temperature-strain curve was measured and recorded by an IR camera, showing a consistent temperature cycling stability over 100 cycles from approximately 90.3 to 89.7 °C. The corresponding minimum temperature difference that can be detected is 0.6 °C, and by combining the previous linear fitting function in eq (11), we can obtain a formula on the strain change ($\Delta\varepsilon$), as follows:

$$(7.03 \times 10^{-4}) / \% \Delta\varepsilon = 1/89.7 - 1/90.3 \quad (12)$$

Thus $\Delta\varepsilon = 0.105\%$ (13)

, which indicates that the strain resolution is $\sim 0.105\%$, which shows an outstanding wireless strain sensitivity and high strain resolution of the optimized strain sensor.

Based on the research above, we designed a multichannel strain sensor system consisting of five identical strain sensors operating in a parallel connection, and precisely realized strain detection of individual fingers for an intelligent manipulator. Fig. 5a displays the movements of each finger at approximately the same initial temperature. The temperatures of the four strain sensors attached to the thumb, forefinger, ring finger and little finger were almost unchanged and corresponded to no initial movement of these fingers. The middle finger was then subjected to four levels of strain, firstly increasing and then decreasing, which led to a decrease and an increase of sensor temperature respectively. Supplementary Movie S2 records image of the temperature images at four bending degrees of a middle finger. After the temperatures reached an equilibrium state, the five fingers went through different degrees of bending and a recovery processes in sequence; from thumb to little finger. The temperature variation process was recorded in Supplementary Movie S3. Additionally, Supplementary Fig. S14 indicates the temperature variation and corresponding temperature distribution images. Fig. 5b and 5c present the time-dependent temperature curves of five individual fingers for six cycles under simultaneous finger motion and the enlarged temperature curve indicates the excellent stability of the stretchable strain sensors. Movie S4 illustrates the dynamic temperature variation of the five sensors and Fig. 5d displays the corresponding temperature mapping figures of Fig. 5b at seven stable conditions, and it can be seen that the temperatures of five fingers are all different under every stable states corresponding to different strain.

Discussion

In this article, through a controllable vacuum filtration and precise laser engraving processes, we have fabricated and demonstrated high-performance graphene-ecoflex nanocomposites as stretchable strain sensors with large dimensions (35 mm × 8 mm), and successfully realized wireless monitoring of small strains in intelligent robots based on a strain sensitive Joule heating effect in a controllable direct current power system. The fabricated strain sensor shows excellent cyclic stability of the Joule heating effect over 150 and 400 cycles under repetitive strains from 0 to 100% and 50% respectively. By engineering and optimizing the structure of graphene-polymer nanocomposites, the strain sensitivity of the strain sensor was increased from 3.57×10^{-4} to 7.03×10^{-4} °C⁻¹/% in 0-30% strains range. As a wearable device, the system is able to wirelessly monitor small strain of intelligent robot using an IR camera with an ultra-high strain resolution ~0.1%. Furthermore, we designed five identical strain sensors that operate in a parallel connection to work as a multichannel strain sensor system to precisely realize strain detection of individual finger of an intelligent robot in real time. The research and development of wireless strain detection with high-performance are undoubtedly important for exploring and broadening application scenarios and conditions of flexible strain sensors, which make it a promising candidate for monitoring

strain wirelessly and even remote monitoring of human motion for artificial intelligence fields.

Methods

Materials. Graphene water slurry was purchased from Deyang Carbonene Technology Co., Ltd. The silicone elastomer (ecoflex 0020) was purchased from Shanghai Smarttech Co., Ltd, where the silicone film was achieved by mixing part A and part B with the ratio of 1:1 in weight. All chemicals were used without further purification.

Fabrication of stretchable strain sensors. The synthesis method of graphene-ecoflex nanocomposite film was described similarly in previous work²⁷. To measure the Joule heating effect and strain sensing property, graphene-ecoflex films with dimension of 35 mm × 8 mm were fabricated, and the middle area with the dimension of 20 mm × 8 mm were carved by a laser engraving machine. Two sides of film were fixed on a tense tester with effective dimension of 20 mm × 8 mm of the film suspended. The stretchable strain sensors were applied an external voltage on two sides of the sensor via two Al electrodes.

Characterization and Measurements. The graphene and its nanocomposites were characterized by a field-emission scanning electron microscope (SEM, Hitachi SU8020) and transmission electron microscope (TEM, FEI/Tecnai G2 F20 S-TWIM TMP). The specimens were carved by a laser engraving machine (Universal, PLS 4.75), and the engraving depth was characterized by a profilometer (KLA-Tencor P7). Temperature variations and images were recorded through an IR camera (optris, PI400). The electrical signals were characterised with a Keithely 2611B system controlled by a computer.

References

1. Kim, D. H. *et al.* Epidermal electronics. *Science* **333**, 838-843 (2011).
2. Gao, W. *et al.* Fully integrated wearable sensor arrays for multiplexed in situ perspiration analysis. *Nature* **529**, 509-514 (2016).
3. Cheng, Y., Wang, R., Sun, J., Gao, L. A Stretchable and Highly Sensitive Graphene-Based Fiber for Sensing Tensile Strain, Bending, and Torsion. *Adv. Mater.* **27**, 7365-71 (2015).
4. Yamada, T. *et al.* A stretchable carbon nanotube strain sensor for human-motion detection. *Nat. Nanotech.* **6**, 296-301 (2011).
5. Lipomi, D. J. *et al.* Skin-like pressure and strain sensors based on transparent elastic films of carbon nanotubes. *Nat. Nanotech.* **6**, 788-792 (2011).
6. Chen, X. Y. *et al.* On-Skin Triboelectric Nanogenerator and Self-Powered Sensor with Ultrathin Thickness and High Stretchability. *Small*, **13**, 1702929 (2017).
7. Pu, X. J. *et al.* Eye motion triggered self-powered mechnosensational communication system using

- triboelectric nanogenerator. *Sci. Adv.* **3**, e1700694 (2017).
8. Jung, S. *et al.* Reverse-micelle-induced porous pressure-sensitive rubber for wearable human-machine interfaces. *Adv. Mater.* **26**, 4825-4830 (2014).
 9. Shepherd, R. F. *et al.* Multigait soft robot. *Proc. Natl Acad. Sci. USA* **108**, 20400-20403 (2011).
 10. Morin, S. A. *et al.* Camouflage and display for soft machines. *Science* **337**, 828-832 (2012).
 11. Boutry, C. M. *et al.* A stretchable and biodegradable strain and pressure sensor for orthopaedic application. *Nat. Electron.* **1**, 314-321(2018).
 12. Boutry, C. M. *et al.* Biodegradable and flexible arterial-pulse sensor for the wireless monitoring of blood flow. *Nat. Biomed. Eng.* **3**, 47-57 (2019).
 13. Cheng, X. L. *et al.* Implantable and self-powered blood pressure monitoring based on a piezoelectric thinfilm: Simulated, in vitro and in vivo studies. *Nano Energy* **22**, 453-460 (2016).
 14. Khang, D.-Y., Jiang, H., Huang, Y., Rogers, J. A. A stretchable form of single-crystal silicon for high-performance electronics on rubber substrates. *Science* **311**, 208-212 (2006).
 15. Boland, C. S. *et al.* Sensitive electromechanical sensors using viscoelastic graphene-polymer nanocomposites. *Science* **354**, 1257-1260 (2016).
 16. Li, X. *et al.* Stretchable and highly sensitive graphene-on-polymer strain sensors. *Sci. Rep.* **2**, 870 (2012).
 17. Kim, J. *et al.* Stretchable silicon nanoribbon electronics for skin prosthesis. *Nat. Commun.* **5**, 5747 (2014).
 18. Kim, J. *et al.* Wearable smart sensor systems integrated on soft contact lenses for wireless ocular diagnostics. *Nat. Commun.* **8**, 14997 (2017).
 19. Wang, Y.; Wang, L.; Yang, T.; Li, X.; Zang, X.; Zhu, M.; Wang, K.; Wu, D.; Zhu, H., Wearable and Highly Sensitive Graphene Strain Sensors for Human Motion Monitoring. *Adv. Funct. Mater.* **24**, 4666-4670 (2014).
 20. Hong, S. *et al.* Stretchable Electrode Based on Laterally Combed Carbon Nanotubes for Wearable Energy Harvesting and Storage Devices. *Adv. Funct. Mater.* **27**, 1704353 (2017).
 21. Boland, C. S. *et al.* Sensitive, high-strain, high-rate bodily motion sensors based on graphene-rubber composites. *ACS nano* **8**, 8819-8830 (2014).
 22. Amjadi, M., Pichitpajongkit, A., Lee, S., Ryu, S., Park, I. Highly stretchable and sensitive strain sensor based on silver nanowire-elastomer nanocomposite. *ACS nano* **8**, 5154-5163 (2014).
 23. Geim, A. K., Novoselov, K. S. The rise of graphene. *Nat. Mater.* **6**, 183 (2007).
 24. Castro Neto, A. H. *et al.* The electronic properties of graphene. *Rev. Mod. Phys.* **81**, 109-162 (2009).
 25. Basko, D. A Photothermoelectric Effect in Graphene. *Science* **334**, 610 (2011).
 26. Novoselov, K. S. *et al.* Electric Field Effect in Atomically Thin Carbon Films. *Science* **306**, 666

(2004).

27. Zhang, D., Zhang, K. W., Wang, Y. M., Wang, Y. H., Yang, Y. Thermoelectric effect induced electricity in stretchable graphene-polymer nanocomposites for ultrasensitive self-powered strain sensor system. *Nano Energy* **56**, 25-32 (2019).
28. Liu, Y. *et al.* Solution Adsorption Formation of a pi-Conjugated Polymer/Graphene Composite for High-Performance Field-Effect Transistors. *Adv. Mater.* **30**, 1705377 (2018).
29. Yan, C. *et al.* Highly stretchable piezoresistive graphene-nanocellulose nanopaper for strain sensors. *Adv. Mater.* **26**, 2022-2027 (2014).
30. Dagdeviren, C. *et al.* Conformable amplified lead zirconate titanate sensors with enhanced piezoelectric response for cutaneous pressure monitoring. *Nat. Commun.* **5**, 4496 (2014).
31. Park, D. Y. *et al.* Self-Powered Real-Time Arterial Pulse Monitoring Using Ultrathin Epidermal Piezoelectric Sensors. *Adv. Mater.* **29**, 1702308 (2017).
32. Ota, S., Ando, A., Chiba, D. A flexible giant magnetoresistive device for sensing strain direction. *Nat. Electron.* **1**, 124-129 (2018).
33. Kim, H. W. *et al.* Microwave-Assisted Synthesis of Graphene-SnO₂ Nanocomposites and Their Applications in Gas Sensors. *ACS Appl. Mater. Inter.* **9**, 31667-31682 (2017).
34. Liu, Q.; Chen, J.; Li, Y.; Shi, G., High-Performance Strain Sensors with Fish-Scale-Like Graphene-Sensing Layers for Full-Range Detection of Human Motions. *ACS Nano* **10**, 7901-7906 (2016).
35. Stassi, S., Cauda, V., Canavese, G., Pirri, C. F. Flexible tactile sensing based on piezoresistive composites: a review. *Sensors* **14**, 5296-332 (2014).
36. Lu, N.; Lu, C.; Yang, S.; Rogers, J. Highly Sensitive Skin-Mountable Strain Gauges Based Entirely on Elastomers. *Adv. Funct. Mater.* **22**, 4044-4050 (2012).

Acknowledgments

This work was supported by the National Key R&D Program of China (Grant No. 2016YFA0202701), the National Natural Science Foundation of China (Grant Nos. 51472055), External Cooperation Program of BIC, Chinese Academy of Sciences (Grant No. 121411KYS820150028), the 2015 Annual Beijing Talents Fund (Grant No. 2015000021223ZK32), Qingdao National Laboratory for Marine Science and Technology (No. 2017ASKJ01), the University of Chinese Academy of Sciences (Grant No. Y8540XX2D2), and the "thousands talents" program for the pioneer researcher and his innovation team, China.

Author contributions

Y.Y. conceived the idea and supervised the research; D.Z. and S.X. fabricated the composite materials;

D.Z., S.X., X.Z. and W.Q. carried out the device fabrication and the performance measurement; D.Z., C.R.B., and Y. Y. analyzed the data and co-wrote the manuscript. All the authors read and revised the manuscript.

FIGURES

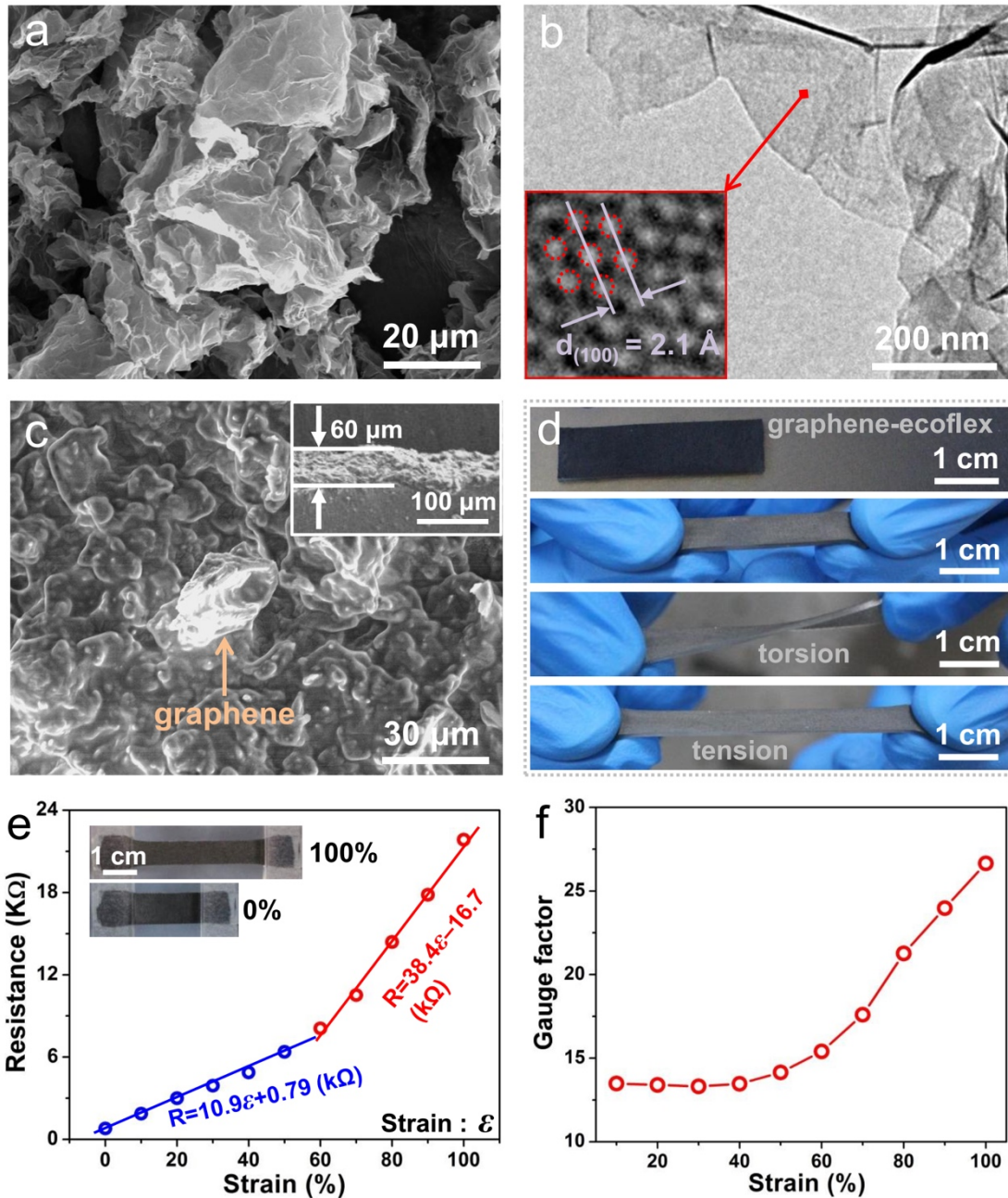


Figure 1. Characterization of graphene sheet and graphene-ecoflex nanocomposite. (a) SEM images of graphene sheets. (b) Low-magnification TEM image of graphene sheet. Inset shows a high-magnification TEM image. (c) SEM images of the graphene-ecoflex nanocomposite film. (d) Photograph of graphene-ecoflex nanocomposite film subjected to different deformation states. (e) Resistance variation of the graphene-nanocomposite film with applied tensile strain from 0 to 100%. Inset: photographs of the film with applied strain of 0 and 100%. (f) The gauge factor variation with the increase of strain from 0 to 100%.

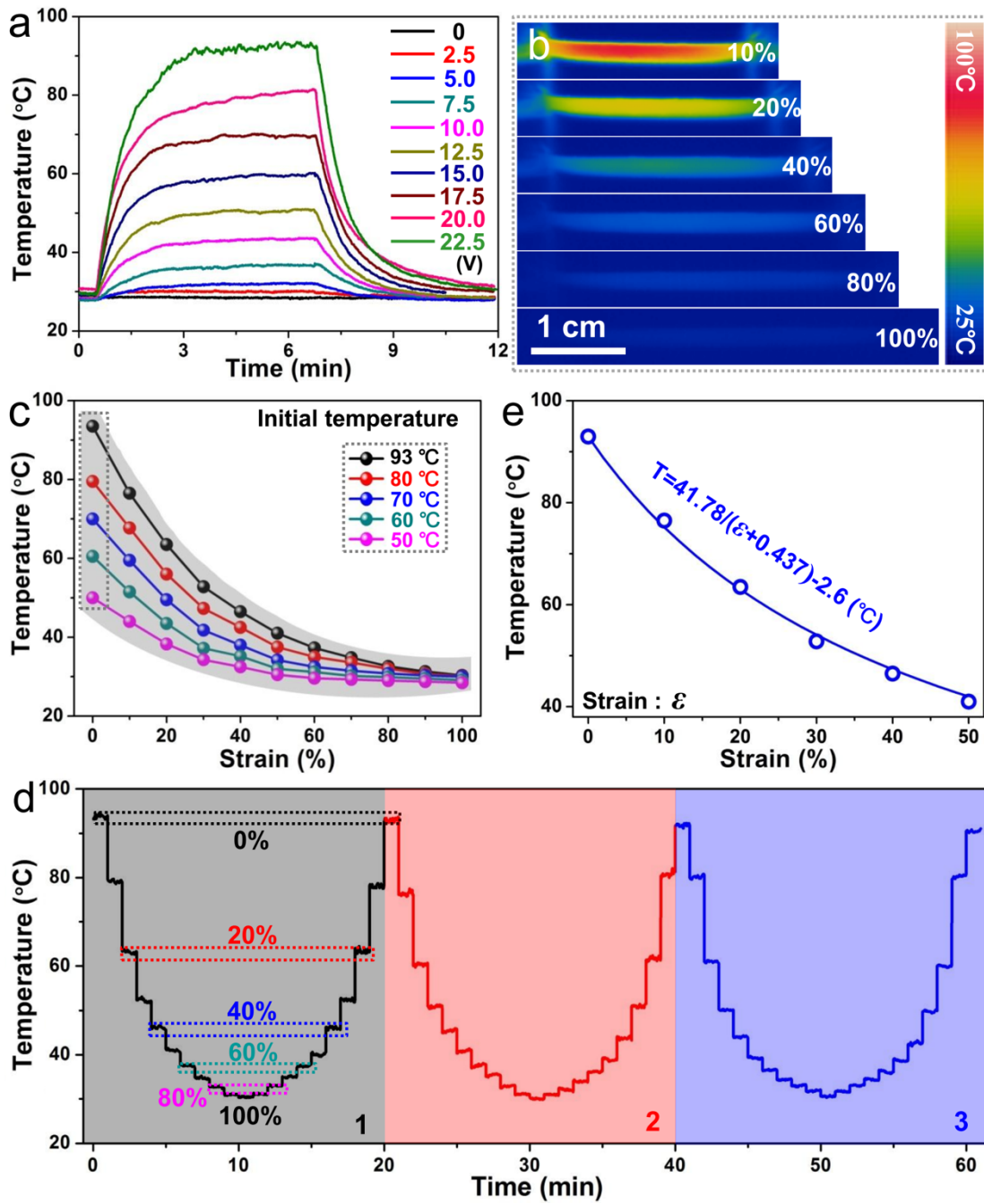


Figure 2. Joule heating effect and cyclic stability. (a) Time-dependent temperature variation with externally applied voltage. (b) Recorded temperature mapping of the film at different strain levels. (c) Temperature changes of five initial temperatures and strain from 0 to 100%. (d) Three cycle tests of consecutively stretching/releasing process, a 0-100% strain. (e) Fitting function of the temperature variation with initial temperature of 93 °C.

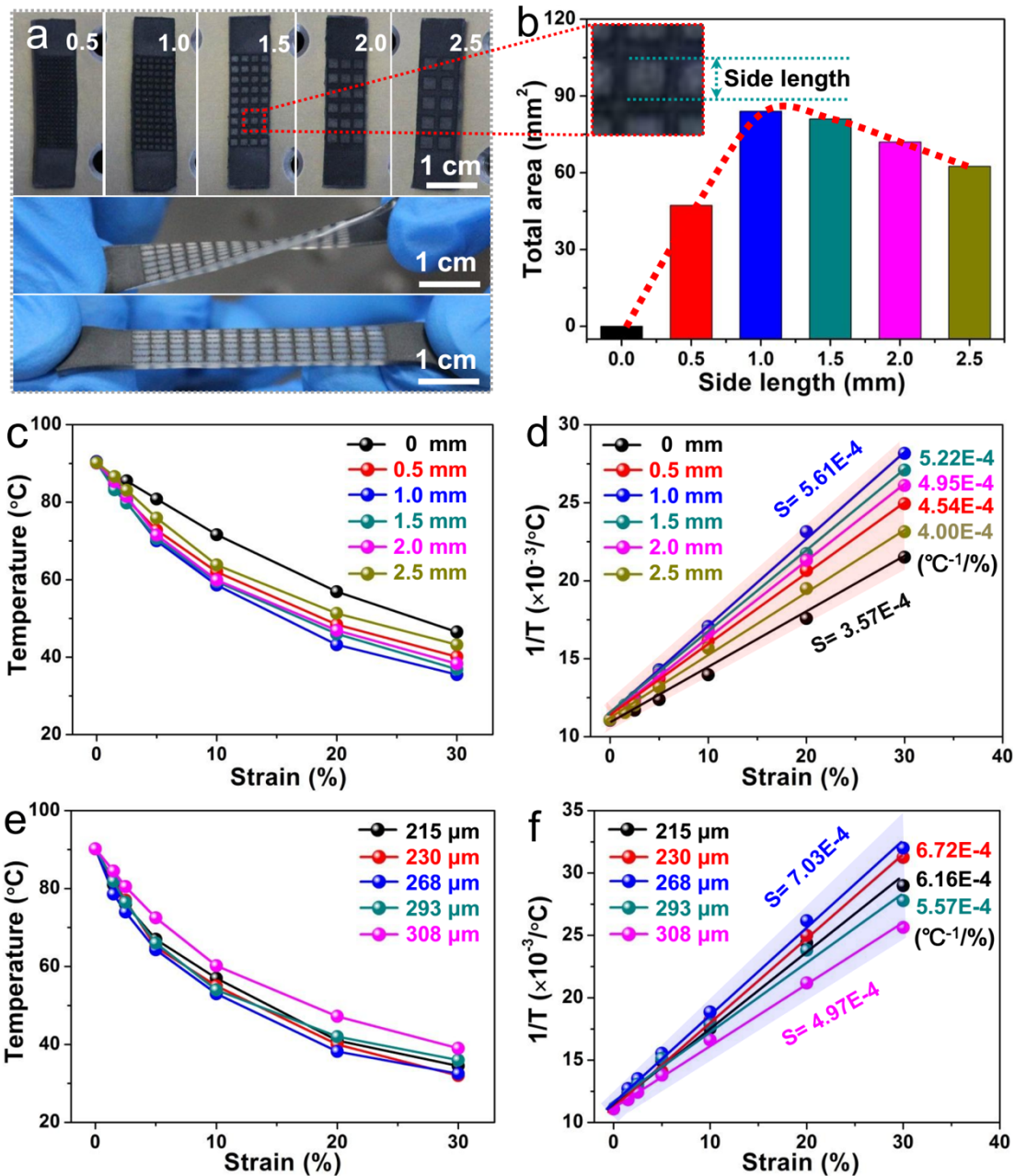


Figure 3. Strain sensing property of the stretchable strain sensor. (a,b) Photograph of graphene-ecoflex film with different engraving side length (a) and corresponding graphene-free total areas (b). (c) The temperature-strain curves for the fifth cycle of the six specimens with different engraving side length. (d) Linear fitting curves between $1/T$ and strain, ε , corresponding to (c). (e) Temperature-strain curves for the fifth cycle of the five specimens with different engraving depth. (f) Linear fitting curves between $1/T$ and ε corresponding to (e).

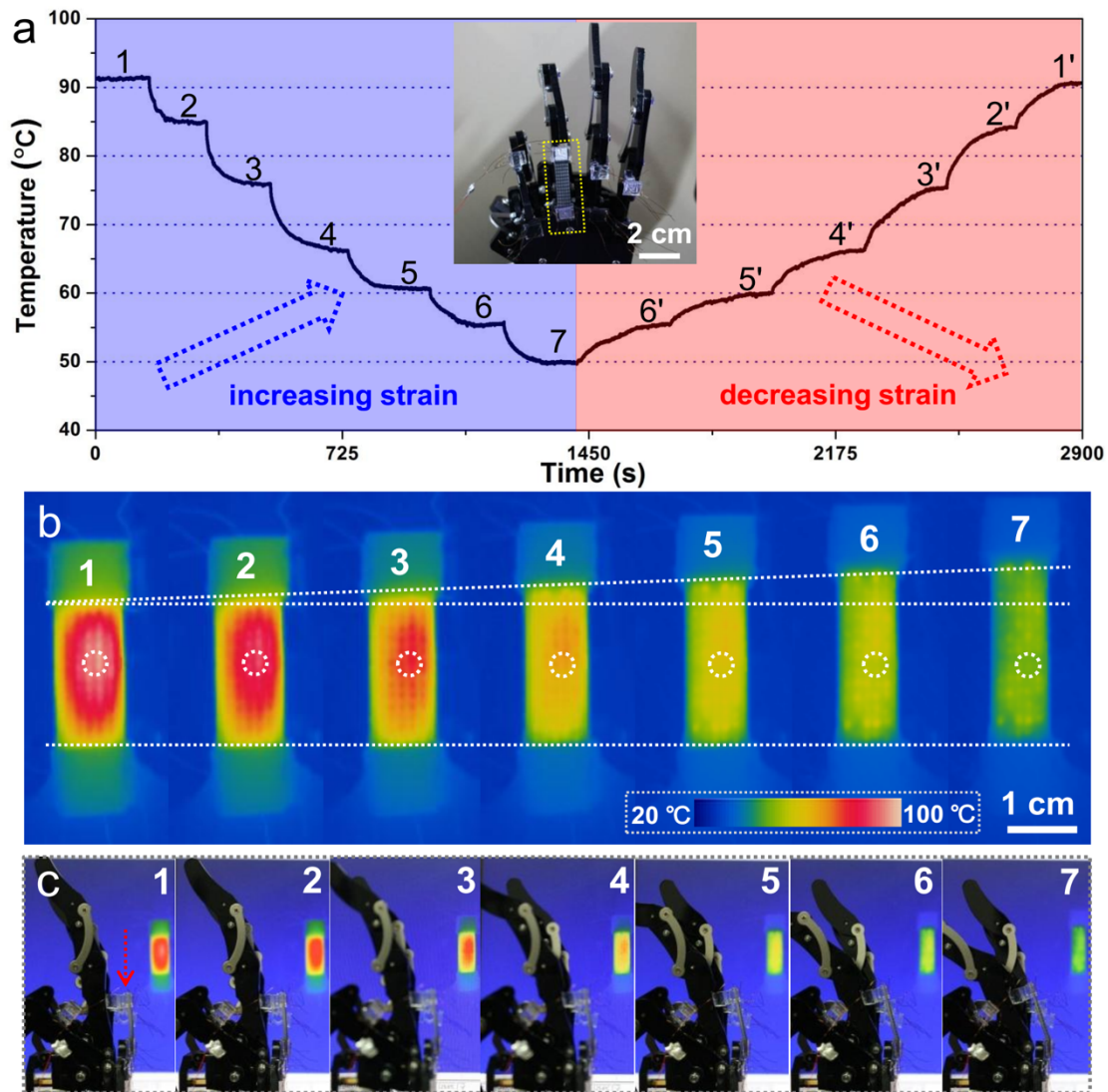


Figure 4. Strain-induced temperature variation of the strain sensor for wireless monitoring of finger motion. (a) Temperature variation with gradually increasing strain and corresponding recovery process. Insert is a photograph of the manipulator test device. (b,c) Seven different temperature distribution images (b) and photographs (c) of the manipulator, corresponding to the seven bend states of the finger in (a).

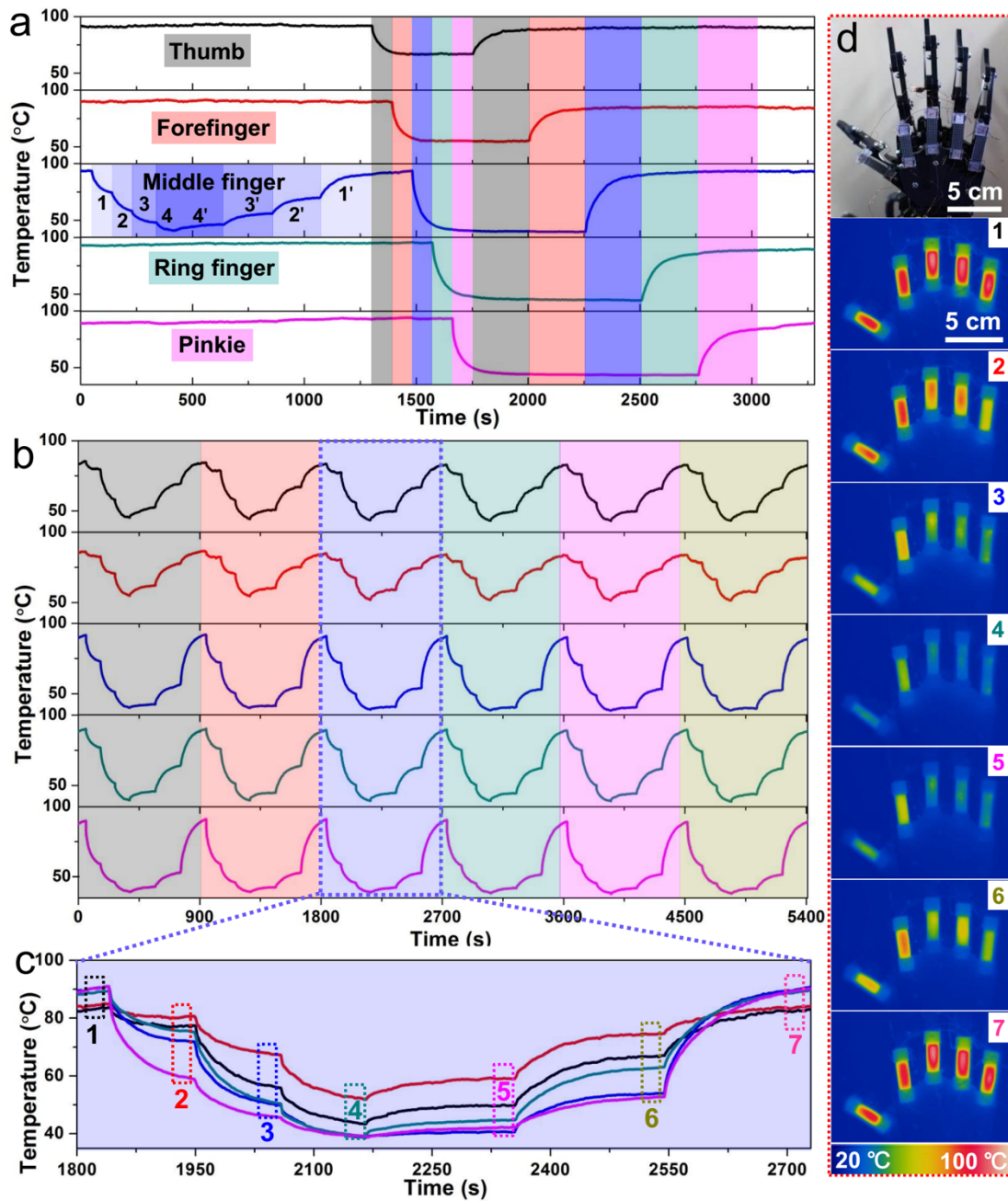


Figure 5. Application for wireless and simultaneous monitoring of the motion of five fingers. (a) Temperature variation with the movement of each finger with the same initial temperature. (b) Five time-dependent temperature curves over six cycles of simultaneous finger motion. (c) Enlarged temperature curve in (b). (d) Photograph and corresponding temperature mapping of figures under different states of motion in (b).

